Int. J. Electrochem. Sci., 7 **(2012)** 2349 - 2360

International Journal of
ELECTROCHEMICAL
SCIENCE
www.electrochemsci.org

Effect of Ceftezole on the Corrosion of Mild Steel in HCl Solution

Ashish Kumar Singh [*], *Eno E. Ebenso*

Department of Chemistry, School of Mathematical and Physical Sciences, North-West University (Mafikeng Campus), Private Bag X2046, Mmabatho 2735, South Africa
[*]E-mail: ashish.singh.rs.apc@itbhu.ac.in

Received: 10 February 2012 / *Accepted:* 24 February 2012 / *Published:* 1 March 2012

The adsorption and corrosion inhibition behaviour of ceftezole (CFZ) at mild steel surface were studied gravimetrically and electrochemically by using electrochemical impedance spectroscopy (EIS) and Tafel polarization techniques. The increase in concentration, immersion time and temperature shows a positive effect on inhibition efficiency. Inhibitor molecules directly adsorb on the surface on the basis of donor acceptor interactions between the p-electrons of benzene, sulphur and nitrogen atoms and the vacant d-orbitals of iron atoms. The adsorption of CFZ followed Langmuir adsorption isotherm. Potentiodynamic polarization study revealed that CFZ acted as mixed type of inhibitor. The results obtained from different methods are in good agreement.

Keywords: Corrosion inhibition; Langmuir adsorption; Kinetic parameters; Polarization

1. INTRODUCTION

Using inhibitors is one of the most practical methods for protecting metals against corrosion, especially in acidic media [1]. Many industrial processes such as acid cleaning bath, water cooling system, various refinery operations, pipelines, chemical operations, steam generators, ballast tanks, oil and gas production units are involved with inhibitors due to high corrosion rates in these parts. Most of the commercial inhibitors are toxic in nature; therefore, their replacement by environmentally benign inhibitors is necessary. Recently, a few non-toxic compounds such as cefazolin [2], ceftobiprole [3], disulfiram [4], cefuroxime [5], diethyl carbamazine [6], and ceftazidime [7] have been studied as corrosion inhibitors.

In a continuation of our research, the inhibition effect of ceftezole (CFZ) on the corrosion of mild steel (MS) in 1 M HCl solution was studied using weight loss, potentiodynamic polarization curves and electrochemical impedance spectroscopy (EIS) methods.

Ceftezole is a cephalosporin antibiotic. It is the commercial name of (6R, 7R) 8-oxo-7-{[2-(tetrazol-1-yl) acetyl] amino} - 3-(1, 3, 4-thiadiazol-2-ylsulfanylmethyl)-5-thia- 1-azabicyclo [4.2.0] oct-2-ene-2-carboxylic acid. The structure of CFZ is presented as Fig. 1.

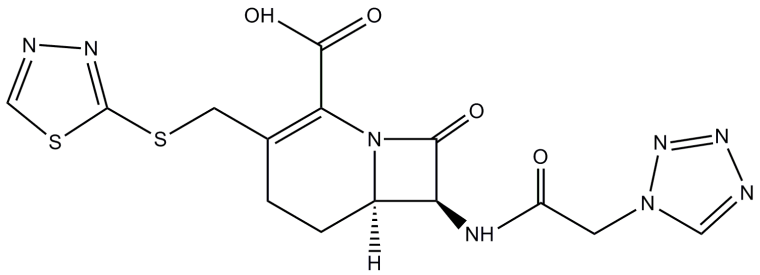

Figure 1. Molecular structure of ceftezole (CFZ)

2. EXPERIMENTAL

2.1. Inhibitor

Stock solution of CFZ was made in 10:1 ratio of water: ethanol mixture to ensure solubility. This stock solution was used for all experimental purposes.

2.2. Mild steel sample

The chemical composition of the working electrode, a mild steel electrode was determined as (wt. %) C = 0.17, Mn = 0.46, Si = 0.26, S = 0.017, P = 0.019 and balance Fe. It was mechanically ground with 320 - 1200 emery grade paper, washed in acetone and bidistilled water then dried and put into the cell.

2.3. Electrochemical measurements

A three-electrode cell consisting of carbon steel working electrode

(WE), a platinum counter electrode (CE) and saturated calomel electrode (SCE) as a reference electrode, was used for electrochemical measurements. All experiments were performed in atmospheric condition without stirring. Prior to the electrochemical measurement, a stabilization period of 30 min was allowed, which was proved to be sufficient to attain a stable value of E_{corr}.

The EIS measurements were carried out in a frequency range from 100 kHz to 0.00001 kHz under potentiodynamic conditions, with amplitude of 10 mV peak-to peak, using AC signal at E_{corr}.

The potentiodynamic polarization curves were recorded in the potential range of -250 to +250 mV (SCE) with scan rate 1 mV s^{-1}. All potentials were measured against SCE.

2.4. Weight loss measurements

Weight loss experiments were done according to the method described previously [8]. Weight loss measurements were performed at 308 K for 3 h by immersing the mild steel coupons into acid solution (100 mL) without and with various amounts of inhibitors. After the elapsed time, the specimen were taken out, washed, dried and weighed accurately.

The inhibition efficiency ($\mu_{WL}\%$) and surface coverage (θ) was determined by using the following equations:

$$\mu_{WL}\% = \frac{w_0 - w_i}{w_0} \times 100 \quad (1)$$

$$\theta = \frac{w_0 - w_i}{w_0} \quad (2)$$

Where, w_0 and w_i are the weight loss value in the absence and presence of inhibitor.

3. RESULTS AND DISCUSSION

3.1 Electrochemical impedance spectroscopy

Impedance method provides information about the kinetics of the electrode processes and simultaneously about the surface properties of the investigated systems. The shape of impedance gives mechanistic information. The method is widely used for investigation of the corrosion inhibition processes [9]. Nyquist plots of mild steel in 1 M HCl solution in the absence and presence of different concentrations of CFP are presented in Fig. 2a. It follows from Fig. 2a that a high frequency (HF) depressed charge-transfer semicircle was observed followed by a well defined inductive loop in the low frequency (LF) regions. The HF semicircle is attributed to the time constant of charge transfer and double-layer capacitance [10, 11]. The LF inductive loop may be attributed to the relaxation process obtained by adsorption species as Cl^-_{ads} and H^+_{ads} on the electrode surface [12]. To get more accurate fit of these experimental data, the measured impedance data were analysed by fitting in to equivalent circuit given in Fig. 2c. The equivalent circuit consists of the double-layer capacitance (C_{dl}) in parallel to the charge transfer resistance (R_{ct}), which is in series to the parallel of inductive elements (L) and R_L. The presence of L in the impedance spectra in the presence of the inhibitor indicates that mild steel is still dissolved by the direct charge transfer at the CFP-adsorbed mild steel surface [13].

One constant phase element (CPE) is substituted for the capacitive element to give a more accurate fit, as the obtained capacitive loop is a depressed semi-circle. The depression in Nyquist semicircles is a feature for solid electrodes and often referred to as frequency dispersion and attributed to the roughness and other inhomogenities of the solid electrode [14]. The CPE is a special element

whose admittance value is a function of the angular frequency (ω), and whose phase is independent of the frequency. The admittance and impedance of CPE is given by;

$$Y_{CPE} = Y_0(i\omega)^n \quad (3)$$

where, Y_0 is the magnitude of CPE, i is an imaginary number ($i^2 = -1$) α is the phase angle of CPE and $n = \alpha/(\pi/2)$ in which α is the phase angle of CPE.

The point of intersection between the inductive loop and the real axis represents ($R_s + R_{ct}$). The electrochemical parameters, Including R_s, R_{ct}, R_L, L, Y_0 and n, obtained from fitting the recorded EIS using the electrochemical circuit of Fig. 2c are listed in Table 1. C_{dl} values derived from CPE parameters according to equation (4) are listed in Table 1.

$$C_{dl} = Y_0(\omega_{max})^{n-1} \quad (4)$$

where, ω_{max} is angular frequency ($\omega_{max} = 2\pi f_{max}$) at which the imaginary part of impedance ($-Z_i$) is maximal and f_{max} is AC frequency at maximum.

Table 1. Electrochemical parameters derived from EIS for mild steel in absence and presence of different concentrations of CFZ

Inhibitor conc. (ppm)	**R_s (Ω cm^2)**	**Q (10^{-6} × Ω^{-1} s^n cm^{-2})**	**n**	**L (H)**	**R_{ct}(Ω cm^2)**	**R_L(Ω cm^2)**	**μ_{R_α} %**
-	1.3	164	0.811	13	16	1	-
100	1.0	54	0.833	1	73	3	78
200	1.0	53	0.855	3	86	5	81
300	1.4	48	0.875	13	231	9	93
400	0.9	42	0.899	73	339	41	95

3.2 Potentiodynamic polarization measurements

Polarization measurements were carried out in order to gain insight into the kinetics of the cathodic and anodic reactions. Fig.2b shows the results of the effect of CFZ concentration on the cathodic and anodic polarization curves of mild steel in 1 M HCl, respectively. It could be observed that both the cathodic and anodic reactions were suppressed with the addition of CFZ, which suggested that the CFZ reduced anodic dissolution and also retarded the hydrogen evolution reaction.

Electrochemical corrosion kinetics parameters, i.e. corrosion potential (E_{corr}), cathodic and anodic Tafel slopes (b_a, b_c) and corrosion current density (i_{corr}) obtained from the extrapolation of the polarization curves, were given in Table 2.

Fig. 2b shows the potentiodynamic polarization curves of mild steel in 1 M HCl in the absence and presence of various concentrations of the CFZ and it is shown that in the presence of the inhibitor,

the curves are shifted to lower current regions, showing the inhibition tendency of the CFZ. There was no definite trend observed in the E_{corr} values in the presence of CFZ. In the present study, maximum shift in E_{corr} values is in the range of 22 mV suggested that CFZ acted as mixed type of inhibitor [2, 4]. The values of various electrochemical parameters derived by Tafel polarization of all the inhibitors are given in Table 1. Investigation of Table 2 revealed that the values of b_a change slightly in the presence of CFZ where as more pronounced change occurs in the values of b_c, indicating that both anodic and cathodic reactions are effected but the effect on the cathodic reactions is more prominent. Thus, CFZ acted as mixed type, but predominantly cathodic inhibitor [7]. Increase in inhibition efficiencies with increasing concentration of CFZ reveals that inhibition action is due to adsorption on steel surface and the adsorption is known to depend on the chemical structure of the inhibitors.

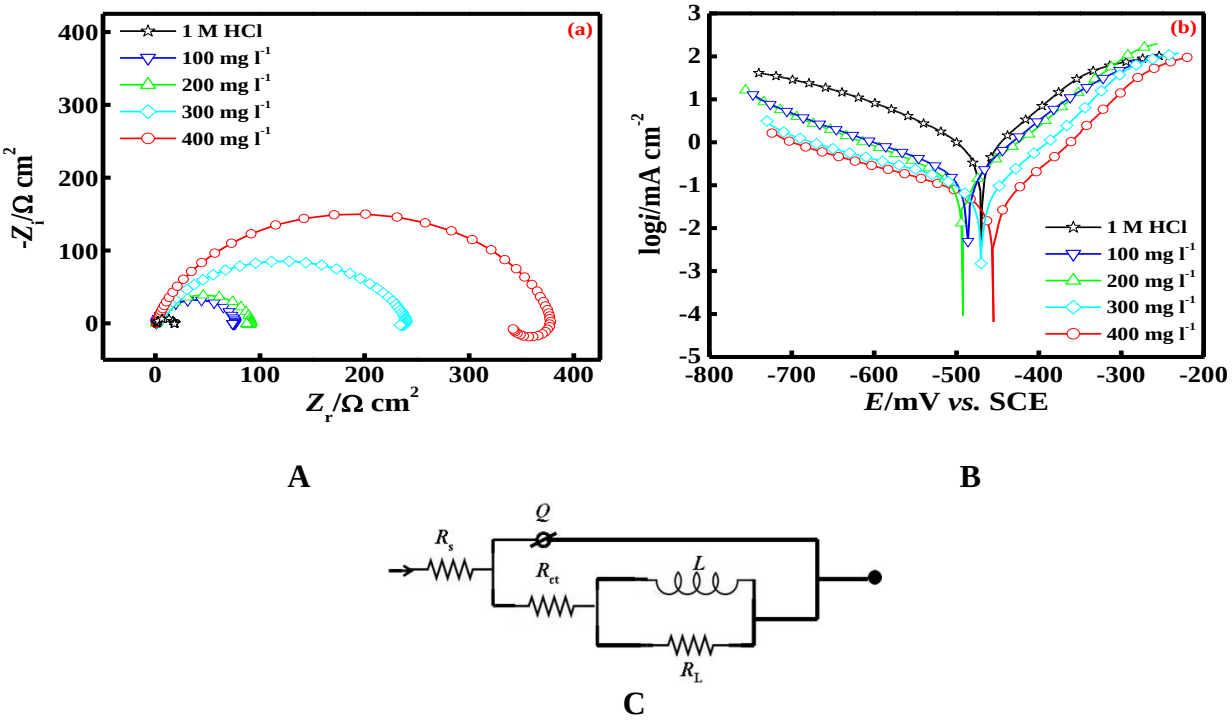

Figure 2. (a) Nyquist plots, (b) Typical polarization curves for corrosion of mild steel in 1 M HCl in the absence and presence of different concentrations of CFP and (c) the electrochemical equivalent circuit used to fit the impedance measurements.

Table 2. Electrochemical parameters derived from Tafel polarization for mild steel in absence and presence of different concentrations of CFZ

$-E_{corr}$ (mV vs. SCE)	i_{corr} (μA cm^{-2})	b_a (mV dec^{-1})	b_c (mV dec^{-1})	μ_p %
469	730	73	127	-
486	212	75	181	71
492	131	72	133	82
469	84	78	165	89
455	37	66	142	95

3.3 Weight loss measurements

3.3.1 Effect of inhibitor concentration

The variation of inhibition efficiency (μ_{WL} %) with inhibitor concentration is shown in Fig.3a. Better inhibition efficiency at higher concentration may be attributed to larger coverage of metal with inhibitor molecules.

3.3.2 Effect of immersion time

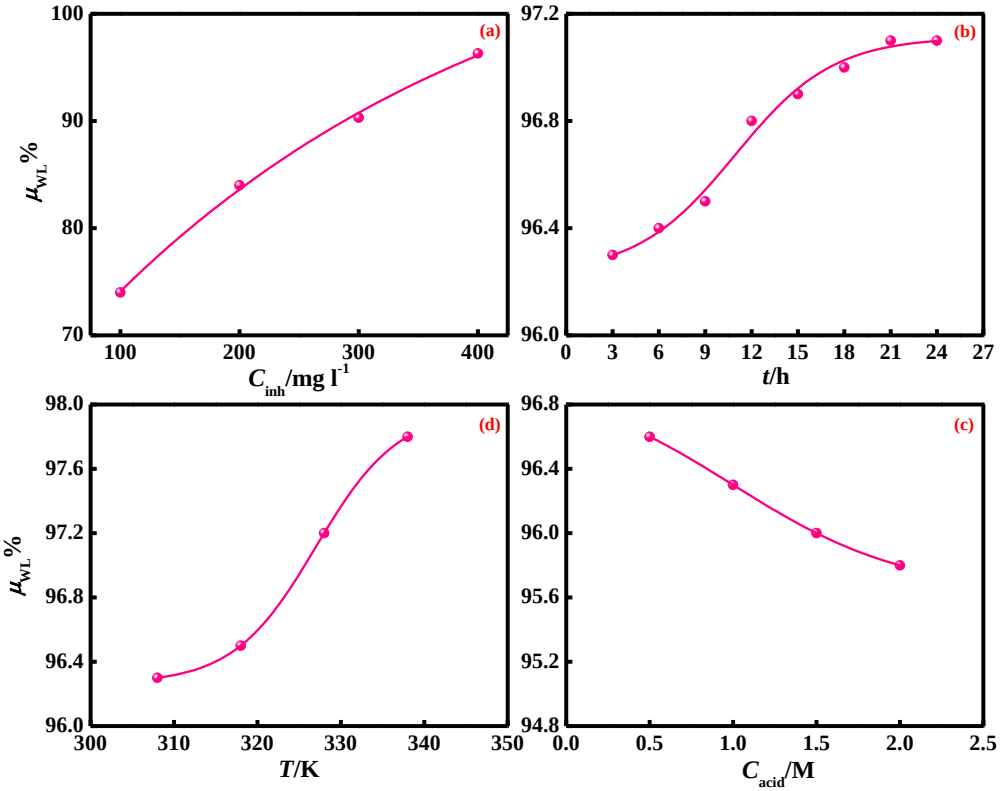

Figure 3. variation of inhibition efficiency with (a) inhibitor conc., (b) immersion time, (c) acid conc. and (d) temperature

From the Fig. 3b, it can be seen that the inhibition efficiency (μ_{WL} %) of inhibitor increased slightly with increasing immersion time up to 18 h but thereafter almost constant meaning that persistent film formation is the function of immersion time.

3.3.3 Effect of acid concentration

The variation of inhibition efficiency (μ_{WL} %) with concentration of acid solution is shown in Fig.3b. It can be seen that CFP acted as an efficient inhibitor in the studied concentration range.

3.3.4 Effect of temperature

The values of inhibition efficiencies obtained from weight loss measurement for the optimum concentration of CFP (400 ppm) in 1 M HCl are shown in Fig.3d. The inhibition efficiency of CFP decreased gradually with increasing temperature.

3.4 Thermodynamic activation parameters

In order to calculate the activation parameters of the corrosion process and investigate the mechanism of inhibition, weight loss measurements were performed in the temperature range of 303-338 K in the absence and presence of 400 mg l^{-1} concentrations of CFZ solutions.

The dependence of corrosion rate on temperature can be expressed using the Arrhenius equation and transition state equation

$$\log(C_{\mathrm{R}}) = \frac{-E_{\mathrm{a}}}{2.303RT} + \log \lambda \tag{5}$$

$$C_{\mathrm{R}} = \frac{RT}{Nh} \exp\left(\frac{\Delta S^{*}}{R}\right) \exp\left(-\frac{\Delta H^{*}}{RT}\right) \tag{6}$$

where E_{a} apparent activation energy, λ the pre-exponential factor, ΔH^{*} the apparent enthalpy of activation, ΔS^{*} the apparent entropy of activation, h Planck's constant and N the Avogadro number, respectively. The apparent activation energy and pre-exponential factors at different concentration of CFZ can be calculated by linear regression between $\log C_{\mathrm{R}}$ and $1/T$ (Fig. 4a); the results were shown in Table 3.

The lowering of activation energy in the presence of inhibitor has been explained in different ways in the literature. Some authors showed that at higher temperatures the surface covered by the inhibitor increases and the rate determining step of the metal dissolution becomes the diffusion through the film of corrosion products and inhibitor. According to other authors [15] the lower activation energy in presence of inhibitor is indication for its chemisorption. The pre-exponential factor λ in the Eq. (5) is related to the number of active centres or sites. In this case, the value of λ in the presence of inhibitor is lower than that for the blank solution. The values of E_{a} and λ decreased in the presence of inhibitor (the higher E_{a} and lower λ led to lower corrosion rate) hence, it was clear that lowering of λ is the decisive factor affecting the corrosion rate of mild steel in 1 M HCl.

Fig. 4b shows the plot of log (C_{R}/T) vs. $1/T$. Straight lines were obtained with a slope equal to ($-\Delta H^{*}/2.303$ R) and intercept equal to [log(R/Nh) + ($\Delta S^{*}/2.303$R)], from which the values of ΔH^{*} and ΔS^{*} were calculated and listed in Table 3. Inspection of these data reveals that the thermodynamic parameters (ΔH^{*} and ΔS^{*}) of dissolution reaction of mild steel in 1 M HCl in presence of CFZ are higher than in the absence of inhibitor. The positive sign of enthalpy reflect the endothermic nature of steel dissolution process meaning that dissolution of steel is difficult [16]. On comparing the values of

the entropy of activation (ΔS^*) given in Table 3, it is clear that entropy of activation decreased in the presence of CFZ indicated that disordering decreased on going from reactant to activated complex.

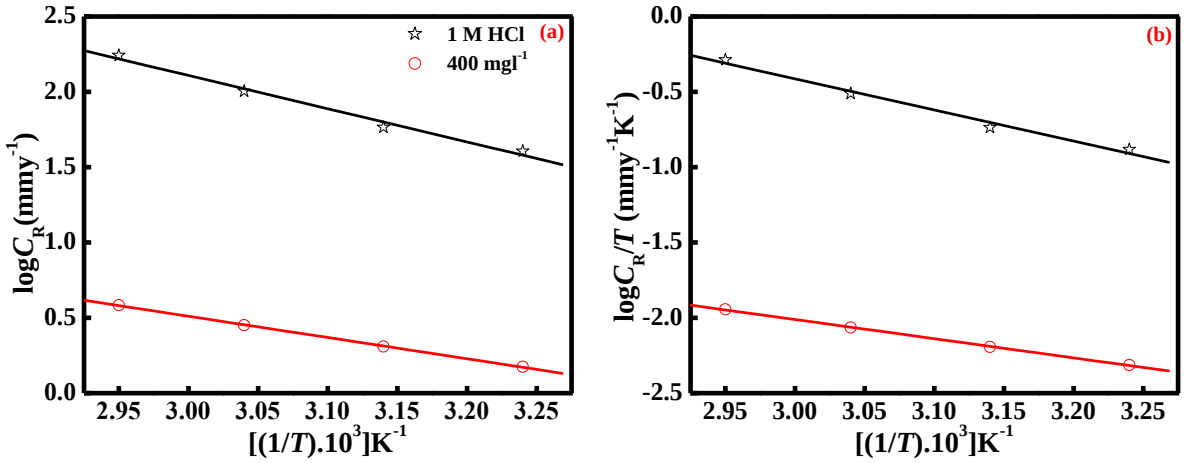

Figure 4. Arrhenius plots in absence and presence of 400 ppm concentration of CFP for (a) log C_R versus 1/T and (b) log (C_R/T) versus 1/T

Table 3. Values of activation parameters for mild steel in 1 M HCl in the absence and presence of 400 mgl^{-1} concentration of CFZ

Inhibitor concentration ($mg\ l^{-1}$)	**E_a ($kJ\ mol^{-1}$)**	**λ (mmy^{-1})**	**ΔH^* ($kJ\ mol^{-1}$)**	**ΔS^* ($J\ K^{-1}\ mol^{-1}$)**
-	42.21	5.3×10^8	39.55	308.42
400	27.02	5.5×10^4	24.37	232.21

3.5 Adsorption isotherm

The adsorption on the corroding surfaces never reaches the real equilibrium and tends to reach an adsorption steady state. When corrosion rate is sufficiently decreased in the presence of inhibitor, the adsorption steady state has a tendency to attain quasi-equilibrium state. Now, it is reasonable to consider quasi-equilibrium adsorption in thermodynamic way using the appropriate adsorption isotherm. The degree of surface coverage (θ) for inhibitor was obtained from average weight loss data. Different adsorption isotherms were tested in order to find the best fitted adsorption isotherm for adsorption of CFZ on the surface of mild steel from 1 M HCl solution. Since, the linear regression coefficient of Langmuir adsorption isotherm is found more close to unity hence, was found best fit. With regard to the Langmuir adsorption isotherm the surface coverage (θ) of the inhibitor on the mild steel surface is related to the concentration (C_{inh}) of the inhibitor in the bulk of the solution according to the following equation:

$$\theta = \frac{K_{ads} C_{inh}}{1 + K_{ads} C_{inh}} \quad (7)$$

where, K_{ads} is the equilibrium constant for the adsorption/desorption process. This equation can be rearranged to

$$\frac{C_{inh}}{\theta} = \frac{1}{K_{ads}} + C_{inh} \quad (8)$$

It is known fact that K_{ads} represents the strength between adsorbate and adsorbent. Large values of K_{ads} imply more efficient adsorption and hence better inhibition efficiency [17].

From the intercepts of the straight lines on the C_{inh}/θ-axis (Fig. 5a), K_{ads} can be calculated which is related to free energy of adsorption, ΔG^{o}_{ads} as given by equation 9.

$$\Delta G^{o}_{ads} = -RT \ln(55.5 K_{ads}) \quad (9)$$

The negative values of ΔG^{o}_{ads} ensure the spontaneity of the adsorption process and stability of the adsorbed film on the mild steel surface [18]. It is usually accepted that the value of ΔG^{o}_{ads} around -20 kJ mol^{-1} or lower indicates the electrostatic interaction between charged metal surface and charged organic molecules in the bulk of the solution while those around -40 kJ mol^{-1} or higher involve charge sharing or charge transfer between the metal surface and organic molecules [19].

Assuming thermodynamic model, corrosion inhibition of mild steel in the presence of CFZ can be better explained, therefore, heat of adsorption and entropy of adsorption were calculated.

According to Van't Hoff equation [20]:

$$\ln K_{ads} = \frac{-\Delta H^{o}_{ads}}{RT} + \text{constant} \quad (10)$$

To calculate heat of adsorption $\ln K_{ads}$ was plotted against $1/T$, as shown in Fig. 5b, straight line was obtained with slope equal to $(-\Delta H^{o}_{ads}/R)$ and intercept equal to $(\Delta S^{o}_{ads}/R + \ln 1/55.5)$. The calculated values of heat of adsorption and entropy of adsorption are listed in Table 4. Under the experimental conditions, the adsorption heat could be approximately regarded as the standard adsorption heat (ΔH^{o}_{ads}).

The thermodynamic parameters ΔH^{o}_{ads} and ΔS^{o}_{ads} can also be calculated from the following equation:

$$\Delta G^{o}_{ads} = \Delta H^{o}_{ads} - T\Delta S^{o}_{ads} \quad (11)$$

A plot of ΔG^{o}_{ads} vs. T gives straight line (Fig. 5c) with the slope equal to $-\Delta S^{o}_{ads}$, and the value of ΔH^{o}_{ads} can be calculated from intercept. Values of ΔH^{o}_{ads} and ΔS^{o}_{ads} obtained by these different methods are in good agreement.

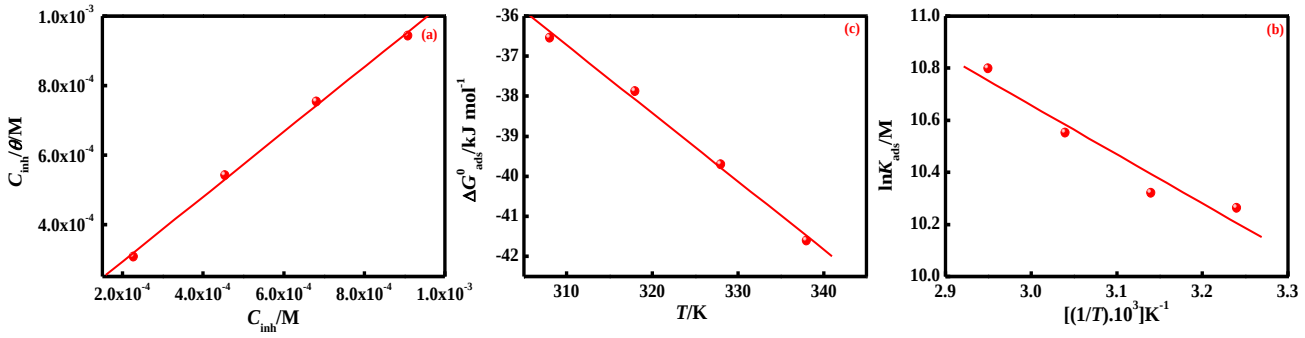

Figure 5. Adsorption isotherm plots for (a) Langmuir isotherm, (b) ln K_{ads} *vs.* 1/*T*, (c) ΔG^{o}_{ads} *vs. T*

Table 4. Thermodynamic parameters for the adsorption of CFZ on the mild steel at 400 mgl^{-1} concentration.

Temperature (K)	ΔG^{0}_{ads} (kJ mol^{-1})	K_{ads} (M × 10^{4})	$^{*}\Delta H^{0}_{ads}$ (kJ mol^{-1})	$^{*}\Delta S^{0}_{ads}$ (J K^{-1} mol^{-1})	$^{\dagger}\Delta H^{0}_{ads}$ (kJ mol^{-1})	$^{\dagger}\Delta S^{0}_{ads}$ (J K^{-1} mol^{-1})
308	-36.55	2.87	-15.65	168.92	-15.90	170.0
318	-37.88	3.04				
328	-39.70	3.82				
338	-41.61	4.90				

4. MECHANISM OF INHIBITION

It has been assumed that organic inhibitor molecule establish its inhibition action via the adsorption of the inhibitor onto the metal surface. The adsorption process is affected by the chemical structures of the inhibitors, the nature and charged surface of the metal and the distribution of charge over the whole inhibitor molecule. In general, owing to the complex nature of adsorption and inhibition of a given inhibitor, it is impossible for single adsorption mode between inhibitor and metal surface.

The adsorption and inhibition effect of CFZ in HCl solution can be explained as follows: CFZ might be protonated in the acid solution as following:

$$CFZ + xH^{+} \leftrightarrow [CFZH_{x}]^{x+} \quad (13)$$

Thus, in aqueous acidic solutions, the CFZ exists either as neutral molecules or in the form of cations (protonated CFZ). Generally, two modes of adsorption could be considered. The neutral CFZ

may be adsorbed on the metal surface via the chemisorption mechanism, involving the displacement of water molecules from the metal surface and the sharing electrons between the N atoms and iron. The CFZ molecules can also be adsorbed on the metal surface on the basis of donor–acceptor interactions between π-electrons of nonbonded electrons of hetero atoms and carbonyl group and vacant d-orbital of iron. Instead of this dπ- dπ bonds are also formed by the overlap of 3d-electrons of Fe-atom to vacant 3d-orbital of S-atom. On another hand, it is well known that the steel surface shows positive charge in acid solution [21], so it is difficult for the protonated CFZ to approach the positively charged steel surface (H_3O^+/metal interface) due to the electrostatic repulsion. Since chloride ions have a smaller degree of hydration, being specifically adsorbed, they create an excess negative charge towards the solution and favour more adsorption of the cations, the protonated CFZ may adsorb through electrostatic interactions between the positively charged molecules and the negatively charged metal surface.

5. CONCLUSIONS

(a) CFZ was found to be a good inhibitor for mild steel corrosion in acid medium.

(b) The inhibition efficiency of CFZ increased with temperature, which leads to a decrease in activation energy of the corrosion process.

(c) EIS results were interpreted using an equivalent circuit in which a constant phase element (*CPE*) including an inductive element (*L*) was used in order to give more accurate fit to the experimental results.

(d) Potentiodynamic polarization curves revealed that CFZ is a mixed-type inhibitor.

ACKNOWLEDGEMENT
AKS is thankful to North West University, South Africa for post doctoral fellowship.

References

1. G. Trabanelli, *Corrosion* 47 (1991) 410.
2. A. K. Singh, M. A. Quraishi, *Corros. Sci.* 52 (2010) 152.
3. A. K. Singh, M. A. Quraishi, *J. Appl. Electrochem.* 40 (2010) 1293.
4. A. K. Singh, M. A. Quraishi, *Corros. Sci.* 53 (2011) 1288.
5. A. K. Singh, E. E. Ebenso, M. A. Quraishi, *Int. J. Electrochem. Sci.* (in press)
6. A. K. Singh, M. A. Quraishi, *Corros. Sci.* 52 (2010) 1529.
7. A. K. Singh, S. K. Shukla, M. Singh, M. A. Quraishi, *Mater. Chem. Phys.* 129 (2011) 68.
8. A. K. Singh, M. A. Quraishi, *Mater. Chem. Phys.* 123 (2010) 666.
9. A. A. Hermas, M. S. Morad, M. H. Wahdan, *J. Appl. Electrochem.* 34 (2004) 95.
10. C. Deslouis, B. Tribollet, G. Mengoli, M. M. Musiani, *J. Appl. Electrochem.* 18 (1988) 374.
11. S. S. Abdel Rehim, H. H. Hassan, M. A. Amin, *Appl. Surf. Sci.*, 187 (2002) 279.
12. A. K. Singh, M. A. Quraishi, *Corros. Sci.* 52 (2010) 1373.
13. V. P. Singh, P. Singh, A. K. Singh, *Inorg. Chim. Acta* (2011), doi:10.1016/j.ica.2011.09.037
14. M. Mahadavian, M. M. Attar, *Corros. Sci.* 48 (2006) 4152.

15. A. Popova, M. Christov, A. Vasilev, *Corros. Sci.,* 49, 3276.
16. N. Guan, M. L. Xueming, L. Fei, *Mater. Chem. Phys.,*86 (2004)59.
17. L. Tang, X. Li, Y. Si, G. Mu, G.H. Liu, *Mater. Chem. Phys.* 95 (2006) 26
18. H. Keles, M. Keles, I. Dehri, O. Serindag, *Colloids Surf. A: Physicochem. Eng. Aspects* 320 (2008) 138
19. F. Bentiss, C. Jama, B. Mernari, H. El Attari, L. El Kadi, M. Lebrini, M. Traisnel, M. Lagrenée, *Corros. Sci.* (2009), doi:10.1016/j.corsci.2009.04.009
20. T. P. Zhao, G. N. Mu, *Corros. Sci.* 41 (1999) 1937
21. L. B. Tang, X. Li, L. Li, G. Mu, G. Liu, *Surf. Coat. Technol.* 201 (2006) 384.